applied optics

Refraction index sensor based on phase resonances in a subwavelength structure with double period

DIANA C. SKIGIN[1,2,*] AND MARCELO LESTER[3]

[1]Universidad de Buenos Aires, Facultad de Ciencias Exactas y Naturales, Departamento de Física, Grupo de Electromagnetismo Aplicado, Buenos Aires, Argentina
[2]Universidad de Buenos Aires, Consejo Nacional de Investigaciones Científicas y Técnicas, Instituto de Física de Buenos Aires (IFIBA), Facultad de Ciencias Exactas y Naturales, Buenos Aires, Argentina
[3]Instituto de Física Arroyo Seco, IFAS (UNCPBA) and CIFICEN (UNCPBA-CICPBA-CONICET), Grupo Óptica de Sólidos-Elfo, Pinto 399, 7000 Tandil, Argentina
*Corresponding author: dcs@df.uba.ar

Received 24 June 2016; revised 26 August 2016; accepted 6 September 2016; posted 8 September 2016 (Doc. ID 269093); published 30 September 2016

In this paper, we numerically demonstrate a refraction index sensor based on phase resonance excitation in a subwavelength-slit structure with a double period. The sensor consists of a metal layer with subwavelength slots arranged in a bi-periodic form, separated from a high refraction index medium. Between the metallic structure and the incident medium, a dielectric waveguide is formed whose refraction index is going to be determined. Variations in the refraction index of the waveguide are detected as shifts in the peaks of transmitted intensity originated by resonant modes supported by the compound metallic structure. At normal incidence, the spectral position of these resonant peaks exhibits a linear or a quadratic dependence with the refraction index, which permits us to obtain the unknown refraction index value with a high precision for a wide range of wavelengths. Since the operating principle of the sensor is due to the morphological resonances of the slits' structure, this device can be scaled to operate in different wavelength ranges while keeping similar characteristics.

OCIS codes: (050.6624) Subwavelength structures; (280.1415) Biological sensing and sensors; (050.0050) Diffraction and gratings; (050.2230) Fabry-Perot.

http://dx.doi.org/10.1364/AO.55.008131

1. INTRODUCTION

In recent papers, we investigated in detail the optical response of a system formed by a slotted metallic layer near a dielectric interface [1,2]. We have shown that this structure allows the coupling of the incident wave with the resonant modes of the structure, thus producing enhanced transmission. On the other hand, it is well known that double-period slit structures support phase resonances, which are characterized by a huge intensification of the electromagnetic field within the slits, and simultaneously produce remarkable variations in the spectral transmitted response [3–6]. The narrow gaps or minima that appear within the transmission bands are due to the complex behavior of the electromagnetic fields within the slits. For particular parameters of the structure, highly enhanced transmission peaks with very narrow bandwidths can be obtained for propagation as well as for evanescent illumination [2]. These features make this system a promising candidate for a refraction index sensor with very particular properties.

In the last 20 years, broad research has been done in the field of refraction index sensors and biosensors for detecting DNA, different types of cancer cells and biomolecules or viruses, and molecules. Due to their high sensitivity, devices based on plasmonic excitations have mostly been explored. A very complete and detailed listing of different plasmonic sensors and their comparative characteristics and applications is given in [7]. Plasmonic sensors use the interaction of the evanescent field of a surface plasmon with different structures such as metallic planar films, diffraction gratings, metastructures, nanoparticles, etc. This interaction produces a shift of the plasmon resonance frequency, which is typically detected as an angular shift of a minimum in specular reflectivity. The sensitivity of a surface plasmon sensor is limited fundamentally by the short decay length of the surface plasmons of ~20 μm, which leads to a broad spectral or angular width of the optical signal. Recently, other alternatives have also been explored for the design of refraction index sensors based on a different resonance mechanism [8,9].

Morphological resonances such as phase resonances in systems with double-period slits have been proposed for a large variety of applications such as high finesse optical filters, light trapping and guiding structures [10,11], corrugated surface antennas [12], channel-selecting devices, actively controlled nano-optic devices, and even enhanced SPP sensors [13]. In addition, metallo-dielectric structures similar to those investigated in the present work have been proposed for a variety of applications that range from sensors [14] and quantum well infrared photodetectors to guided mode resonant filters, tailorable thermal emitters, and asymmetric transmission systems [15,16]. In particular, phase resonances seem to be highly sensitive to small refraction index variations and do not depend on the generation of surface waves on specific metals as plasmonic resonances do. These features make dual-period slit systems excellent candidates for use as refraction index sensors. Moreover, the phase resonance phenomenon is scalable with the wavelength in a wide range of the electromagnetic spectrum, and thus exploring the idea of a sensor based on such a mechanism looks to be an attractive and worthwhile endeavor.

The organization of this paper is as follows. In Section 2, we introduce the structure considered and summarize the modal method employed to solve the diffraction problem. In Section 3, we introduce examples that illustrate the general features of the transmitted response of dual-period metallo-dielectric structures in order to highlight their singular properties that offer unique characteristics for sensing applications. Examples of sensor designs are shown in Section 4, where we analyze the evolution of different resonant peaks as a function of the refraction index and evaluate the performance of the sensor. Finally, remarks and conclusions are given in Section 5.

2. CONFIGURATION OF THE PROBLEM AND METHOD

Figure 1 shows a scheme of the sensor, which comprises a dual-period metallic grating near a dielectric interface. The dual-period structure is formed by metallic wires separated by slits. Each period d comprises J subwavelength wires of width a and $J+1$ subwavelength slits of width c (in the scheme of Fig. 1, we considered $J=2$); the height h of the wires is also indicated. The system is illuminated from the medium of refraction index n_1 by a p-polarized plane wave of wavelength λ_0 in a vacuum forming an angle θ_0 with the y axis. The array is separated a distance e from the interface between region 1 and region 2 (refraction index n_2). Thus, the gap of thickness e between the array and the interface forms a waveguide whose refraction index n_2 is going to be determined. Region 3 is the slits' zone (refraction index n_3), and the transmission medium is region 4 with refraction index n_4. All the media are non-magnetic ($\mu_j=1$), meaning that $n_j=\sqrt{\epsilon_j}$, where ϵ denotes the dielectric permittivity and $j=1,\ldots,4$ denotes the region.

To solve the diffraction problem, we apply the modal method, which has been extended to deal with compound gratings [3] and also with structures near a dielectric interface [17]. Taking advantage of the invariance of the problem along the z direction, the full vectorial problem can be separated into two scalar problems corresponding to the basic polarization modes: s (electric field perpendicular to the plane of incidence) and p (electric field parallel to the plane of incidence). In this paper, we consider a p-polarized incident wave. Basically, we apply the modal method developed for highly conducting dual-period wire gratings [3] and extend it to allow an additional dielectric interface.

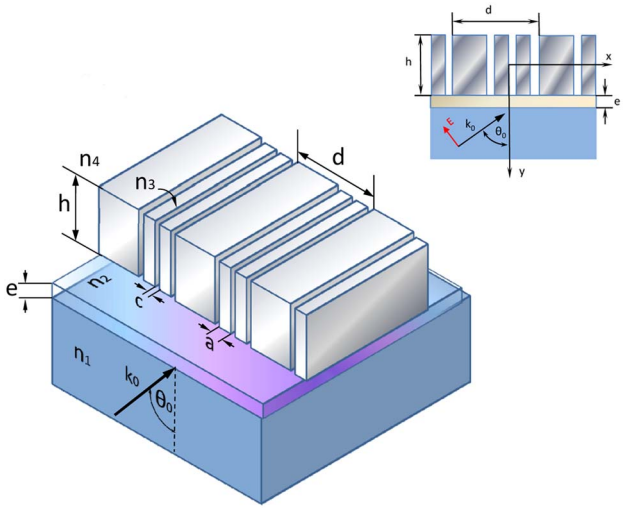

Fig. 1. Scheme of the diffraction problem under study. A p-polarized plane wave of wavelength λ_0 in vacuum impinges with an angle θ_0 on the planar interface between regions 1 (n_1) and 2 (n_2). The dual-period structure has period d, thickness h, and J subwavelength wires within each period (in this scheme, $J=2$), and is separated a distance e from the interface between regions 1 and 2. The slits' width c and the wires' width a are also indicated.

The method consists of dividing the spatial domain into regions and expanding the fields in each region into their own eigenfunctions. In this case, the four regions are separated by the horizontal interfaces at $y=y_{\text{int}}=h/2+e$ (between regions 1 and 2), $y=h/2$ (between regions 2 and 3), and $y=-h/2$ (between regions 3 and 4). In region 1, we have the incident plane wave and the reflected field, and in region 4, we have the transmitted field. Then, the tangential magnetic field in these regions is expressed as

$$H_{z1}(x,y)=\exp[i(\alpha_0 x-\beta_{01}(y-y_{\text{int}}))]+\sum_n R_n\exp[i(\alpha_n x+\beta_{n1}(y-y_{\text{int}}))], \quad (1)$$

$$H_{z4}(x,y)=\sum_n T_n\exp[i(\alpha_n x-\beta_{n4}(y+h/2))], \quad (2)$$

where

$$\alpha_n=k_0 n_1\sin\theta_0+n\frac{2\pi}{d}, \quad (3)$$

$$\beta_{nj}^2=k_0^2 n_j^2-\alpha_n^2,\qquad j=1,\ldots,4, \quad (4)$$

where θ_0 is the angle of incidence, $k_0=2\pi/\lambda_0$, n is an integer that denotes the diffraction order, and R_n and T_n are the unknown reflected and transmitted Rayleigh amplitudes, respectively.

In region 2, the electromagnetic field is represented by upward and downward plane waves

$$H_{z2}(x,y) = \sum_n A_n \exp[i(\alpha_n x - \beta_{n2}(y - h/2))] + \sum_n B_n \exp[i(\alpha_n x + \beta_{n2}(y - h/2))]. \quad (5)$$

Within the slits (region 3), the fields are expanded in terms of the eigenfunctions of a planar waveguide that take into account the boundary conditions on the lateral walls of each slit. Since the proposed sensor is based on phase resonance excitation, the metal is required to be highly conducting, which is obtained at long wavelengths. Therefore, to find the eigenfunctions of the slits' region, we apply the surface impedance boundary condition (SIBC) [18] in order to account for the metal without computing the electromagnetic fields within it. Thus, the field in region 3 is

$$H_{z3}(x,y) = \sum_m U_m(x - x_j) V_{mj}(y), \qquad x_j \le x \le x_j + c; \quad j = 1, \ldots, J+1, \quad (6)$$

where

$$U_m(x - x_j) = \cos[u_m(x - x_j)] + \frac{\eta}{u_m} \sin[u_m(x - x_j)], \quad (7)$$

$$V_{mj}(y) = a_{mj} \cos(v_m y) + b_{mj} \sin(v_m y), \quad (8)$$

$$v_m^2 = k_0^2 - u_m^2, \quad (9)$$

where $\eta = i/(\sqrt{\epsilon_{\text{metal}}} k_0)$, x_j denotes the x coordinate of the left edge of the jth slit, and u_m form the set of solutions of the equation

$$\tan u_m c = \frac{2\eta u_m}{u_m^2 - \eta^2}, \quad (10)$$

which results from the application of the SIBC on the lateral walls of each slit, assuming a vacuum filling, i.e., $n_3 = 1$.

The field expansions given in Eqs. (1), (2), (5), and (6) are matched at the horizontal interfaces $y = \pm h/2$ and $y = y_{\text{int}}$ by imposing the boundary conditions. This imposition produces a system of equations that, after being projected into convenient bases, leads to a matrix equation for the unknown reflected and transmitted amplitudes of the form

$$\begin{pmatrix} M_{11} & M_{12} \\ M_{21} & M_{22} \end{pmatrix} \begin{pmatrix} T \\ R \end{pmatrix} = \begin{pmatrix} I_1 \\ I_2 \end{pmatrix}. \quad (11)$$

The explicit expressions of the matrix elements and the independent vector components are given in Appendix A.

Once the reflected and transmitted amplitudes are found, the far field intensity can be computed. The efficiency of the nth transmitted diffraction order e_n is defined as

$$e_n = |T_n|^2 \frac{\epsilon_1}{\epsilon_4} \frac{\beta_{n4}}{\beta_{01}}, \quad (12)$$

for $\beta_{n4} \in \mathbf{R}$. Then, the total transmitted efficiency T is

$$\mathrm{T} = \sum_n e_n. \quad (13)$$

For practical reasons, we will consider a sensor operating at normal incidence; that is, the incident wave impinges normally onto the planar interface at $y = 0$. Since the source and the detector are aligned, this configuration provides a high degree of symmetry and reduces the technological difficulties that might arise if a specific incidence angle is required, as it occurs in other sensors based on angle-dependent phenomena.

3. GENERAL FEATURES OF THE TRANSMITTED RESPONSE

It is well known that a regular metallic array of 1D subwavelength slits exhibits enhanced transmission for particular resonant wavelengths and that the two physical mechanisms underlying this phenomenon are surface plasmon excitations and coupling to waveguide modes of the slits [19,20]. Recently, it has been shown that if the slits are distributed so as to form a dual-period structure, phase resonances can also take place, which can significantly modify its electromagnetic response [3,6]. In this section, we illustrate the basic characteristics of the transmitted response of a dual-period slit structure near a dielectric interface as an introduction to the refraction index sensor.

In Fig. 2, we show curves of total transmitted efficiency T as a function of λ/d for a structure with $J = 0$ (regularly periodic structure) and $J = 2$ (three slits per period), $c/d = a/d = 0.08$, $h/d = 1.3$, $e/d = 0.2$, and $n_2 = 1.2$ illuminated under normal incidence. The value of ϵ_{metal} has been chosen so as to

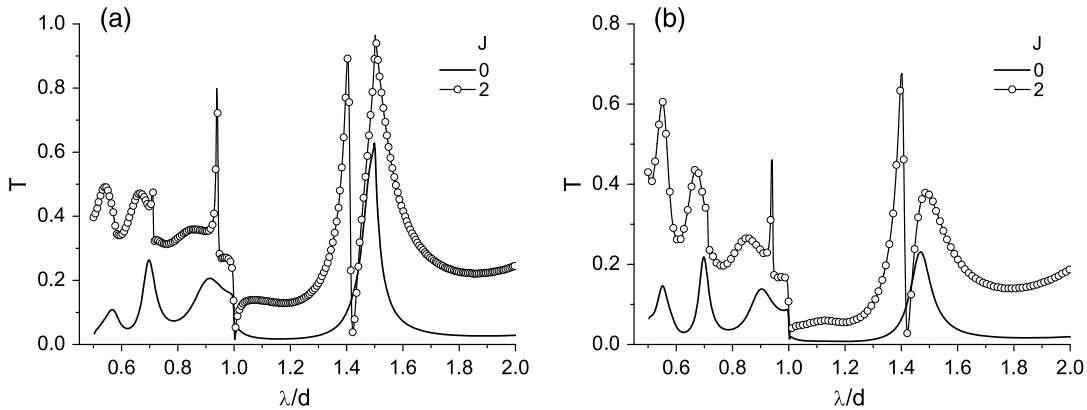

Fig. 2. Total transmitted efficiency as a function of λ/d at normal incidence for two values of n_1: (a) $n_1 = 1.5$, (b) $n_1 = 3.46$. The rest of the parameters are: $J = 2$, $c/d = a/d = 0.08$, $h/d = 1.3$, $e/d = 0.2$, $n_2 = 1.2$, and $n_3 = n_4 = 1$.

simulate a perfect conductor: $\epsilon_{\text{metal}} = -10^8$. Two values of n_1 are considered: $n_1 = 1.5$ [glass, Fig. 2(a)] and $n_1 = 3.46$ [silicon, Fig. 2(b)]. Transmission peaks can be clearly identified in the $J = 0$ curves at $\lambda/d \approx 1.5$, 0.9, 0.7, and 0.56. These peaks are associated with Fabry–Perot (FP) resonances, which in the ideal case of infinitely thin slits, occur at wavelengths $\lambda_m^{\text{FP}} = 2h/m$, with m as an integer, regardless of the angle of incidence. The peaks in Fig. 2 are slightly shifted to shorter wavelengths with respect to the ideally predicted values. This effect is well known and explained in terms of an effective refraction index produced by the finite width of the slits [21,22].

When the slits' distribution is modified so as to form a dual-period structure, the electromagnetic response of the whole structure is significantly modified. The remarkable changes of the transmitted response are produced by the excitation of phase resonances, which have been studied in the last few years for different geometries and illumination conditions [3–6]. In this case, a narrow gap opens up within each FP peak, which splits the resonance into two narrower and more intense peaks. The physical origin of this gap can be explained in terms of phase resonances. In a perfectly periodic grating with a single slit per period, the pseudoperiodic condition implies that the fields in all slits are essentially equal. However, when slits are added to the unit cell, making a compound grating, new degrees of freedom open up since the distribution of field phases in the different slits within a unit cell can have different configurations according to the resonant modes of the system [3]. Under normal incidence, these modes must be symmetrical, and thus the number of possible phase configurations is finite and depends on the number of slits. For three slits in the period, there are only two possible configurations: (i) all the slits have equal phase, or (ii) the external slits have equal phase, different from the central one. In particular, when the phases in adjacent slits within a period are all opposite to each other, π resonances can be excited. Phase resonances are usually generated within a FP mode resonance. For one slit in the period ($J = 0$), different phases in adjacent slits cannot occur, and therefore no phase resonance is present. For $J = 2$, the π mode can be excited, which is why a dip splits each FP resonance into two peaks.

In Fig. 2(a), it can be observed that the peak at $\lambda/d \approx 1.5$ for $J = 0$ is split into two peaks found at $\lambda/d \approx 1.4$ and 1.5; also, the peak at $\lambda/d \approx 0.9$ is divided into two: a broader peak at $\lambda/d \approx 0.85$ and a higher quality one at $\lambda/d \approx 0.93$. The same effect is observed in Fig. 2(b) for $n_1 = 3.46$.

The examples of Fig. 2 illustrate how the different resonant mechanisms present in dual-period structures can eventually be combined to produce an optimized response for a desired application. However, it is important to note that high conductivity of the metal is required to achieve such resonant behavior, which implies operation wavelengths at the far infrared or longer. In the next section, we show how phase resonances can be exploited for the design of a novel refraction index sensor.

4. DUAL-PERIOD STRUCTURE AS A REFRACTION INDEX SENSOR

As mentioned above, the proposed system can be used as a refraction index sensor, which permits detection of differences between the refraction index of a sample and that of a reference material. The substance with unknown refraction index (n_2) might be liquid or solid. According to Fig. 1, the structure admits the inclusion of a medium with refraction index n_3 within the slits and another with n_4 in the transmission region. From the experimental point of view, this means that the slits might be filled by a solid dielectric material that confines the unknown medium (n_2) within the waveguide region. Even though in the examples we consider $n_3 = n_4 = 1$, the introduction of a dielectric medium in regions 3 and 4 would not qualitatively affect the performance of the device.

In order to evaluate the sensitivity of the proposed sensor to small changes of the refraction index of the material within the waveguide (n_2), we focus in two different spectral regions and analyze the evolution of the resonant transmission peaks as n_2 is varied. Taking advantage of the peak splitting produced by phase resonance excitation, the proposed sensor comprises a metallic layer with three slits per period, which produces higher quality resonant peaks than usual single-slit-per-period structures. We evaluate the performance of the sensor for the two incidence media considered in Fig. 2, i.e., optical glass ($n_1 = 1.5$), and $n_1 = 3.46$, which approaches the refraction index of silicon at the near infrared range. In both cases, we focus on the resonant peaks found at $\lambda/d \approx 0.93$ (FP mode $m = 3$) and at $\lambda/d \approx 1.4$ (FP mode $m = 2$).

In Fig. 3, we show total transmitted efficiency curves as a function of the normalized wavelength for different values of the waveguide thickness e. Figure 3(a) corresponds to $n_1 = 1.5$ and $n_2 = 1.2$, and Fig. 3(b) corresponds to $n_1 = 3.46$ and $n_2 = 1.5$. For clarity, the curves corresponding to different values of e/d are shown vertically displaced in one unit. The normalized wavelength range considered in both parts of Fig. 3 covers the FP resonances already observed in Fig. 2. It can be noticed that the resonant peaks stay nearly at the same wavelengths as the waveguide thickness is varied. This gives evidence that the resonant mechanism is not related to waveguide resonances of the slab of refraction index n_2. On the other hand, we have verified that the spectral position of the resonances is highly dependent on the thickness of the periodic metallic structure (h), and this confirms that these resonances are related to mode excitations within the subwavelength slits. Consequently, the waveguide thickness e is not a critical parameter for the sensor design, and it could be chosen according to specific practical purposes related to the material whose refraction index is going to be determined. The possibility of freely choosing the waveguide thickness is one of the advantages of the proposed sensor.

In order to evaluate the performance of the proposed structure as a refraction index sensor, we analyze the spectral location of the resonant peak λ_{res}/d as a function of the relative refraction index of the waveguide $n_{\text{wg}} = n_2/n_4$. It is convenient to introduce the normalized sensitivity s, which permits a quantitative assessment of the variation of the normalized spectral position of the resonant peak with n_{wg}. Then, s is a dimensionless quantity defined as

$$s = \frac{d(\lambda_{\text{res}}/d)}{d n_{\text{wg}}}. \tag{14}$$

In Figs. 4 and 5, we show contour plots of total transmitted efficiency as a function of λ/d and n_{wg} for a structure with $J = 2$, $c/d = a/d = 0.08$, $h/d = 1.3$, $n_3 = n_4 = 1$, and

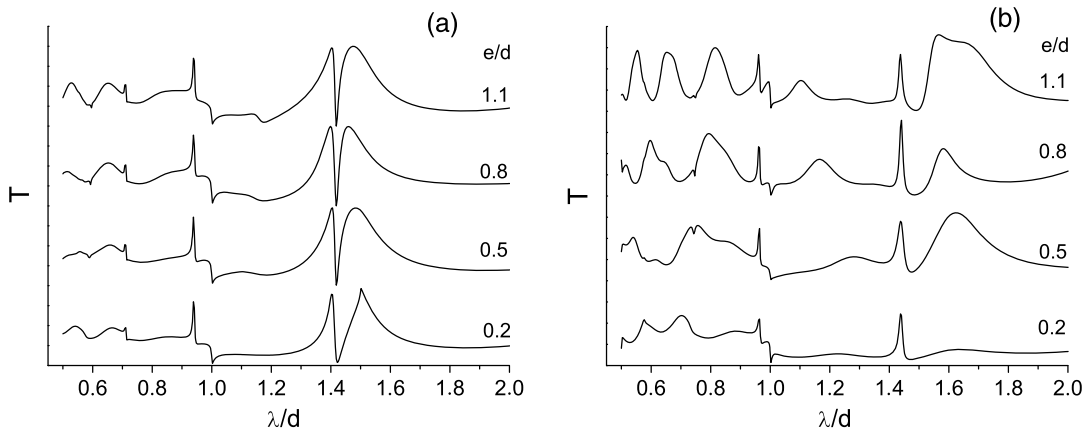

Fig. 3. Total transmitted efficiency as a function of λ/d for different values of e/d:0.2, 0.5, 0.8, and 1.1: (a) $n_1 = 1.5$ and $n_2 = 1.2$, (b) $n_1 = 3.46$ and $n_2 = 1.5$. The rest of the parameters are: $J = 2$, $c/d = a/d = 0.08$, $n_3 = n_4 = 1$, and $\theta_0 = 0°$. For clarity, the curves in each panel are vertically displaced.

$\theta_0 = 0°$. In Fig. 4, $e/d = 0.5$ and $n_1 = 1.5$, and in Fig. 5, $e/d = 0.8$ and $n_1 = 3.46$. In both figures, we analyze three bands that correspond to the $m = 2$ and $m = 3$ FP resonances. The circles correspond to the data points taken into account for the fitting curves (solid lines).

For the $m = 3$ FP resonance ($\lambda_{res}/d \approx 0.93$), the dependence of the resonant wavelength on the refraction index of the waveguide is almost linear, as evidenced by the fitting curve, which corresponds to a linear approximation. This linear behavior implies a constant normalized sensitivity within the refraction index range explored, which takes the values $s = 0.074$ in Fig. 4 and $s = 0.088$ in Fig. 5. The fact that the normalized sensitivity does not depend on a specific wavelength range but rather on the wavelength-to-period ratio constitutes one of the main advantages of the proposed sensor: the size and dimensions of the system can be tailored to meet the requirements of each particular application. Then, the spectral shift between the resonant peaks corresponding to refraction index values that differ in Δn is $\Delta\lambda_{res} = s\Delta n d$. For instance, if $\Delta n = 0.013$ (1% of 1.3) and $d = 1250$ nm, $\Delta\lambda_{res} = 1.2$ nm for the configuration of Fig. 4 and $\Delta\lambda_{res} = 1.43$ nm for the configuration of Fig. 5. The standard sensitivity S, which for this sensor is given by $S = sd$, is $S = 92.5$ nm/refractive index unit (RIU) for the case of Fig. 4 and $S = 110$ nm/RIU for the case of Fig. 5.

In the vicinity of the $m = 2$ FP resonance of the slits, the phase resonance generates a transmission gap of minimum transmittance and splits the FP resonant peak into two [2], as already observed in Fig. 2. The spectral locations of these two resonant peaks follow different behaviors as the refraction index is varied. In both cases (Figs. 4 and 5), the higher energy band peak (shorter wavelengths) can be approximated by a linear function, whereas the lower energy band peak (longer wavelengths) follows a quadratic law. Note that the range of n_{wg} is different in each figure. According to Eq. (14), a sensor based on the shift of the higher energy band peak would exhibit a constant normalized sensitivity $s = 0.104$ for $n_1 = 1.5$ (Fig. 4) and $s = 0.136$ for $n_1 = 3.46$ (Fig. 5). These sensitivity values are higher than those of the $m = 3$ FP resonance and allow for a higher accuracy in the determination of the unknown refraction index. For the same example mentioned above, in this case $\Delta\lambda_{res} = 1.69$ nm and $S = 130$ nm/RIU

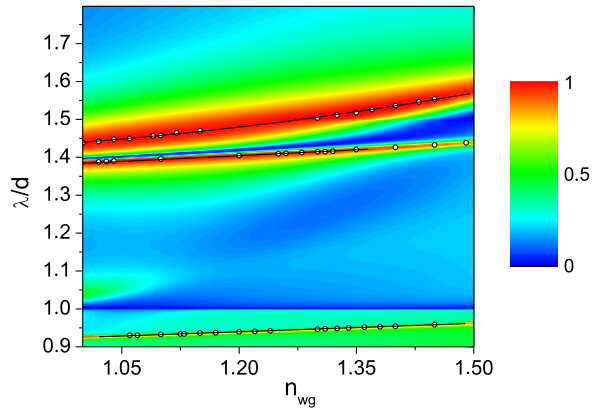

Fig. 4. Contour plot of the total transmitted efficiency as a function of λ/d and n_{wg} for $J = 2$, $c/d = a/d = 0.08$, $h/d = 1.3$, $e/d = 0.5$, $n_1 = 1.5$, $n_3 = n_4 = 1$, and $\theta_0 = 0°$.

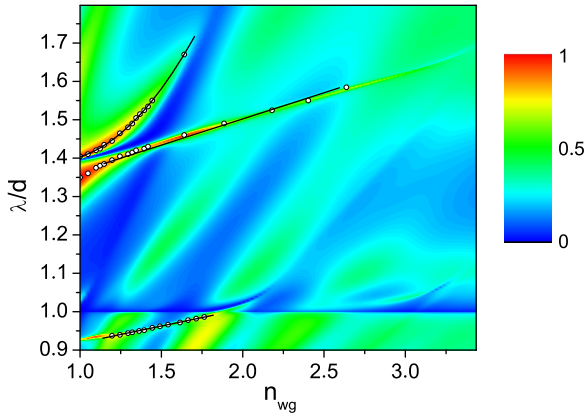

Fig. 5. Contour plot of the total transmitted efficiency as a function of λ/d and n_{wg} for $J = 2$, $c/d = a/d = 0.08$, $h/d = 1.3$, $e/d = 0.8$, $n_1 = 3.46$, $n_3 = n_4 = 1$, and $\theta_0 = 0°$.

for the configuration of Fig. 4, and $\Delta\lambda_{res} = 2.21$ nm and $S = 170$ nm/RIU for the configuration of Fig. 5.

The picture is different at the lower energy band peak of the $m = 2$ FP resonance, at which the dependence of the resonant wavelength with n_{wg} is approximately given by

$$\lambda_{res}/d = s_2 n_{wg}^2 + s_1 n_{wg} + s_0. \quad (15)$$

Therefore, the spectral shift corresponding to a refraction index difference Δn is given by

$$\Delta\lambda_{res} = (2s_2 n_{wg} + s_1)\Delta n d. \quad (16)$$

Taking into account that $s_2 = 0.203$ and $s_1 = -0.243$ for the fitting curve of Fig. 4, for $\Delta n = 0.013$, $n_{wg} = 1.3$, and $d = 1250$ nm, the results are $\Delta\lambda_{res} = 4.63$ nm and $S = 353.5$ nm/RIU. For the configuration of Fig. 5 with $s_2 = 0.44$ and $s_1 = -0.75$, and with the same Δn, n_{wg}, and d, the results are $\Delta\lambda_{res} = 6.4$ nm and $S = 492.5$ nm/RIU. These sensitivity values are significantly higher than those obtained for the $m = 3$ FP resonance and are comparable to the values reported in [7] for other sensors. Furthermore, unlike other sensors, the sensitivity of the proposed sensor depends on the period of the slits' structure, i.e., it increases for increasing d (which implies a proportional increment of the operating wavelength as well). Also, the Q factors of these resonance peaks are very high and reach the value of 60, which also enable a high sensing performance [23]. The existence of two different regimes (linear and quadratic) makes the sensor more versatile. Even though from the practical point of view, a linear relationship between the unknown index and the peak wavelength is usually more convenient, the quadratic dependence, on the other hand, rapidly increases the sensitivity at long wavelengths.

It is important to note that the proposed sensor presents a wider range of applications in comparison with those based on surface plasmon resonances. In addition, the scalability is advantageous from the point of view of the sensor manufacturer because it permits fabrication of the device at the easiest scale that is suitable for the particular sensing purpose. However, taking into account that phase resonances arise at dual-period systems of slits ruled on a highly conducting metal, the spectral range of application of this sensor starts at the near infrared and extends to longer wavelengths, at which the electromagnetic response of noble metals is similar to that of a perfect conductor.

5. CONCLUSIONS

A sensor based on phase resonance excitation has been proposed. The design essentially consists of a dual-period metallic structure with subwavelength slits in the vicinity of a dielectric interface. The phase resonances excited in the system produce narrow enhanced transmission peaks that are used to sense the refraction index of the material filling the waveguide formed between the interface and the slits' array. The main advantage that this novel resonant mechanism brings is the scalability of the sensor: the operation wavelength must be chosen in accordance with the period of the metallic structure, and this period can be selected in order to simplify the manufacture of the device. We have shown that the sensitivity of this sensor is sufficiently high for a variety of applications. One of them is the detection of contaminants in certain substances, as for instance, water. By detecting the spectral position of the peak of a sample of water and comparing it with the reference (clean) signature, the peak shift permits detection of non-desired components within the sample such as heavy metals or organic matter.

Although we investigated the case of a dual-period structure comprising three slits per period, it is to be expected that the sensor sensitivity would still improve if more slits are added within each period because it has already been shown that the addition of slits increases the number of resonances, which also become spectrally narrower. Prior to fabrication of a sensor based on phase resonance excitation, the limitations introduced by noise in the detected signal should be carefully analyzed. As experimentally demonstrated for similar structures [6], it is expected that a few cells would be enough to reproduce the obtained results. To achieve better performance for molecular sensing, the geometrical parameters of the proposed sensor could be adapted to combine phase resonances and the infrared vibrational modes of molecules. In conclusion, phase resonance excitation is a promising mechanism to be exploited for sensing purposes.

APPENDIX A: EXPLICIT EXPRESSIONS OF THE MATRIX ELEMENTS AND THE INDEPENDENT VECTOR OF EQ. (11)

$$M_{11ln} = \delta_{ln} + \frac{\epsilon_4}{\beta_{l4}}\left(\frac{1}{\epsilon_3}\mathcal{C}_{ln}^{-} + \mathcal{B}_{ln}\right), \quad (A1)$$

$$M_{12ln} = -\frac{\epsilon_4}{\epsilon_3}\frac{1}{\beta_{l4}}K_n^{+}\mathcal{C}_{ln}^{+}, \quad (A2)$$

$$M_{21ln} = -\frac{\epsilon_2}{\epsilon_3}\frac{1}{\beta_{l2}}\mathcal{C}_{ln}^{+}, \quad (A3)$$

$$M_{22ln} = -\delta_{ln}K_l^{-} + \frac{\epsilon_2}{\beta_{l2}}K_n^{+}\left(\frac{1}{\epsilon_3}\mathcal{C}_{ln}^{-} + \mathcal{B}_{ln}\right), \quad (A4)$$

$$I_{1l} = \frac{\epsilon_4}{\epsilon_3}\frac{1}{\beta_{l4}}J_0^{+}\mathcal{C}_{l0}^{+}, \quad (A5)$$

$$I_{2l} = \delta_{l0}J_l^{-} - \frac{\epsilon_2}{\beta_{l2}}J_0^{+}\left(\frac{1}{\epsilon_3}\mathcal{C}_{l0}^{-} + \mathcal{B}_{l0}\right), \quad (A6)$$

and

$$\mathcal{C}_{ln}^{\pm} = \frac{i}{2}\sum_j e^{i(\alpha_n-\alpha_l)x_j}\sum_m \frac{v_m}{F_m}\mathcal{A}_{lm}^{-}\mathcal{A}_{nm}^{+}(D_{1m} \pm D_{2m}), \quad (A7)$$

$$\mathcal{B}_{ln} = i\eta\left\{\sum_{j=1}^{J}\int_{x_j+c}^{x_{j+1}} e^{i(\alpha_n-\alpha_l)x}dx + \int_{x_{J+1}+c}^{d} e^{i(\alpha_n-\alpha_l)x}dx\right\}, \quad (A8)$$

$$\mathcal{A}_{nm}^{\pm} = \int_0^c U_m e^{\pm i\alpha_n x}dx, \quad (A9)$$

$$J_l^{\pm} = \frac{1}{2}\{\gamma_l^{+}e^{i\beta_{l2}e} \pm \gamma_l^{-}e^{-i\beta_{l2}e}\}, \quad (A10)$$

$$K_l^{\pm} = \frac{1}{2}\{\gamma_l^- e^{i\beta_{l2}e} \pm \gamma_l^+ e^{-i\beta_{l2}e}\}, \quad \text{(A11)}$$

$$F_m = \int_0^c U_m^2(x)\mathrm{d}x, \quad \text{(A12)}$$

$$D_{1m} = \cot(v_m h/2), \quad \text{(A13)}$$

$$D_{2m} = \tan(v_m h/2), \quad \text{(A14)}$$

$$\gamma_l^{\pm} = 1 \pm \frac{\epsilon_2 \beta_{l1}}{\epsilon_1 \beta_{l2}}. \quad \text{(A15)}$$

Funding. Consejo Nacional de Investigaciones Científicas y Técnicas (CONICET) (PIP 11220110100451); Universidad Nacional del Centro de la Provincia de Buenos Aires (UNICEN); Universidad de Buenos Aires (UBA) (UBACyT 20020150100028B).

Acknowledgment. D. S. gratefully acknowledges support from CONICET and M. L. gratefully acknowledges support from UNICEN. The authors would like to thank the reviewers for their valuable comments, which enhanced our paper.

REFERENCES

1. D. C. Skigin and M. Lester, "Enhanced transmission via evanescent-to-propagating conversion in metallic nanoslits: role of Rayleigh anomalies," J. Opt. **16**, 045004 (2014).
2. M. Lester and D. C. Skigin, "Striking properties of light transmitted by a double period nanoslit structure under evanescent incidence," J. Opt. **17**, 055601 (2015).
3. D. C. Skigin and R. A. Depine, "Transmission resonances in metallic compound gratings with subwavelength slits," Phys. Rev. Lett. **95**, 217402 (2005).
4. D. C. Skigin and R. A. Depine, "Narrow gaps for transmission through metallic structured gratings with subwavelength slits," Phys. Rev. E **74**, 046606 (2006).
5. A. P. Hibbins, I. R. Hooper, M. J. Lockyear, and J. R. Sambles, "Microwave transmission of a compound metal grating," Phys. Rev. Lett. **96**, 257402 (2006).
6. M. Navarro-Cía, D. C. Skigin, M. Beruete, and M. Sorolla, "Experimental demonstration of phase resonances in metallic compound gratings with subwavelength slits in the millimeter wave regime," Appl. Phys. Lett. **94**, 091107 (2009).
7. A. S. M. Z. Kausar, A. W. Reza, T. A. Latef, M. H. Ullah, and M. E. Karim, "Optical nano antennas: state of the art, scope and challenges as a biosensor along with human exposure to nano-toxicology," Sensors **15**, 8787–8831 (2015).
8. J. H. Schmid, W. Sinclair, J. García, S. Janz, J. Lapointe, D. Poitras, Y. Li, T. Mischki, G. Lopinski, P. Cheben, A. Delge, A. Densmore, P. Waldron, and D.-X. Xu, "Silicon-on-insulator guided mode resonant grating for evanescent field molecular sensing," Opt. Express **17**, 18371–18380 (2009).
9. E. Sader and A. Sayyed-Ahmad, "Design of an optical water pollution sensor using a single-layer guided-mode resonant filter," Photonic Sens. **3**, 224–230 (2013).
10. A. Enemuo, M. Nolan, Y. U. Jung, A. B. Golovin, and D. T. Crouse, "Extraordinary light circulation and concentration of *s*- and *p*-polarized phase resonances," J. Appl. Phys. **113**, 014907 (2013).
11. Y. Liang, W. Peng, M. Lu, and S. Chu, "Narrow-band wavelength tunable filter based on asymmetric double layer metallic grating," Opt. Express **23**, 14434–14445 (2015).
12. I. Bendoym, A. B. Golovin, and D. T. Crouse, "The light filtering and guiding properties of high finesse resonant compound gratings," Opt. Express **20**, 22830–22846 (2012).
13. X. Zhou, J. Fang, D. Yang, X. Zhao, B. Tang, and Z. Liu, "Optical transmission through compound gold surface relief slit arrays," Opt. Express **22**, 1085–1093 (2014).
14. C. Ge, Z. Guo, Y. Sun, F. Shen, Y. Tao, J. Zhang, R. Li, and L. Luo, "Spatial and spectral selective characteristics of the plasmonic sensing using metallic nanoslit arrays," Opt. Commun. **359**, 393–398 (2016).
15. S. Zanotto, G. Biasiol, L. Sorba, and A. Tredicucci, "Photonic bands and defect modes in metallo-dielectric photonic crystal slabs," J. Opt. Soc. Am. B **31**, 1451–1455 (2014).
16. H. Zhu, F. Li, B. Tang, X. Zang, and C. Jiang, "Asymmetric transmission through metallic grating with dielectric substrate," Opt. Commun. **318**, 41–46 (2014).
17. M. Lester and D. C. Skigin, "Coupling of evanescent s-polarized waves to the far field by waveguide modes in metallic arrays," J. Opt. A **9**, 81–87 (2007).
18. H. Lochbihler and R. A. Depine, "Highly conducting wire gratings in the resonance region," Appl. Opt. **32**, 3459–3465 (1993).
19. J. A. Porto, F. J. García-Vidal, and J. B. Pendry, "Transmission resonances on metallic gratings with very narrow slits," Phys. Rev. Lett. **83**, 2845–2848 (1999).
20. F. J. García-Vidal and L. Martín-Moreno, "Transmission and focusing of light in one-dimensional periodically nanostructured metals," Phys. Rev. B **66**, 155412 (2002).
21. R. Gordon and A. Brolo, "Increased cut-off wavelength for a subwavelength hole in a real metal," Opt. Express **13**, 1933–1938 (2005).
22. R. Gordon, "Light in a subwavelength slit in a metal: propagation and reflection," Phys. Rev. B **73**, 153405 (2006).
23. R. Singh, W. Cao, I. Al-Naib, L. Cong, W. Withayachumnankul, and W. Zhang, "Ultrasensitive terahertz sensing with high-*Q* Fano resonances in metasurfaces," Appl. Phys. Lett. **105**, 171101 (2014).